

The relationship of loss, mean age of air and the distribution of CFCs to stratospheric  
circulation and implications for atmospheric lifetimes

A. R. Douglass<sup>1</sup>, R. S. Stolarski<sup>1</sup>, M. R. Schoeberl<sup>1</sup>, C. H. Jackman<sup>1</sup>, M. L. Gupta<sup>1,4</sup>,  
P. A. Newman<sup>1</sup>, J. E. Nielsen<sup>2,3</sup>, E. L. Fleming<sup>3</sup>

November 5, 2007

<sup>1</sup>Atmospheric Chemistry and Dynamics Branch, Code 613.3, NASA Goddard Space  
Flight Center, Greenbelt, Maryland, USA

<sup>2</sup>Global Modeling and Assimilation Office, Code 610.1, NASA Goddard Space Flight  
Center, Greenbelt, Maryland, USA

<sup>3</sup>Science Systems and Applications, Inc., Lanham, Maryland, USA

<sup>4</sup>Present Affiliation, Federal Aviation Administration, Washington, DC, USA

1   **Abstract**

2   Projections of the recovery of the ozone layer are made with global atmospheric models  
3   using a specified time-series of mixing ratios of ozone depleting substances (ODSs) at the  
4   lower boundary. This time-series is calculated using observations, emission rates, and an  
5   estimate for the atmospheric lifetime. ODS destruction and simulated atmospheric-  
6   lifetime vary among models because they depend on the simulated stratospheric transport  
7   and mixing. We investigate the balance between the annual change in ODS burden, its  
8   atmospheric loss, and the annual ODS input to the atmosphere using several models.  
9   Some models reproduce realistic distributions for the mean age of air and some do not.  
10   Models with faster circulations produce ‘young’ distributions for the age of air and fail to  
11   reproduce the observed relationship between the mean age of air at a particular location  
12   and the amount of ODS at that location relative to its initial value (i.e., the fractional  
13   release). Models with realistic mean age of air reproduce this observed relationship.  
14   These models yield a lifetime for  $\text{CFCl}_3$  of ~56 years, longer than the 45 year lifetime  
15   used to project future mixing ratios. The residual circulation of our chemistry climate  
16   model speeds up as climate changes. The lifetime of  $\text{CFCl}_3$  decreases to ~52 years by  
17   2050 due to the circulation change. Use of flux boundary conditions in assessment  
18   models rather than specified mixing ratios would produce simulations in which ODS  
19   evolution is consistent with simulated loss, including the time dependence of the loss due  
20   to circulation change.

21

22

## 1. Introduction

Current ozone assessment efforts have two main goals. The first is to verify that the ozone decreases of the 1980's and 1990's have ceased. The second is to predict the behavior of the ozone layer, as the atmospheric burden of green house gases increases and the concentrations of chlorofluorocarbons (CFCs) decline. The CFC decline is due to cessation of production and continued atmospheric loss mainly through photolysis by ultraviolet radiation in the stratosphere (e.g., Chapter 8 of *Scientific Assessment of Ozone Depletion: 2006* [WMO, 2007, hereafter referred to as WMO2007]). This paper is focused on the second goal, and examines the consistency between the annual change in the integrated atmospheric amount, the computed atmospheric loss and the input of CFCs to the atmosphere implied by the boundary conditions.

The procedures used to produce the timeseries of CFC mixing ratios that are used in assessments are discussed in detail in Chapter 8 of WMO2007. These boundary conditions, specified at the lowest model layer, largely control the time evolution of the atmospheric burden of the source gases (i.e., the total mass of the source gas in the atmosphere) in all assessment models because the variations of the mass of source gases in the stratosphere among the models are small compared with the mass of the source gas in the troposphere. Projections for the recovery of the ozone hole using semi-empirical models also rely on these predicted mixing ratios for chlorine and bromine source gases [e.g., *Newman et al.*, 2006].

44 Mixing ratio boundary conditions have been used in assessments since the late 1980s.  
45 Prior assessments pre-dated international agreements to control CFC production, and  
46 used a combination of emissions and mixing ratios to focus on the ozone change in the  
47 upper atmosphere (e.g., *Atmospheric Ozone 1985: Assessment of our Understanding of*  
48 *the Processes Controlling its present Distribution and Change*, [WMO 1985]). In  
49 contemporary assessment calculations the mixing ratio boundary conditions largely  
50 control the evolution of the mixing ratios of  $\text{Cl}_y$  and its components in the upper  
51 stratosphere where nearly all the CFCs have been destroyed. The time evolution of  $\text{Cl}_y$   
52 depends slightly on the circulation. For example, a more rapid overturning stratospheric  
53 circulation will produce a peak in  $\text{Cl}_y$  a year or two ahead of a slower circulation.  
54  
55 The dependence on the circulation is apparent in the distributions of CFCs and  $\text{Cl}_y$  in the  
56 lower stratosphere. *Waugh et al.* [2007] use CTM simulations using different  
57 meteorological fields, horizontal resolution and upper boundary height to show how  
58 differences in simulated transport and mixing affect the net destruction of the source  
59 gases and the distributions of  $\text{Cl}_y$ . The models shown in Figure 6.8 of WMO2007 use the  
60 same boundary conditions, yet the peak October zonal mean inorganic chlorine ( $\text{Cl}_y$ ) at  
61 50 hPa 80°S exhibits a spread of about 0.75 ppbv (~25%) ignoring outliers.  
62  
63 Despite the difference in the peak amounts of  $\text{Cl}_y$ , its evolution over time is similar  
64 among most of the models. In the WMO2007 models  $\text{Cl}_y$  increases substantially between  
65 1980 and 2000, and decreases by a similar amount between 2005 and about 2050 in direct  
66 response to the imposed mixing ratio boundary conditions. Here we show that the

constraint on the overall evolution of the CFCs and  $\text{Cl}_y$  produces inconsistency between the annual change in burden (prescribed by the boundary conditions) and the simulated loss.

In addition to their use in predicting the future mixing ratios of CFCs, atmospheric lifetimes are important to the evaluation of the reservoirs of CFCs called banks. Banks exist because CFCs have commonly been used in closed applications such as refrigeration and air conditioning. As long as the appliances remain operational, the CFCs are sealed and not released to the atmosphere. The magnitude and rate of release of CFCs from these banks are subjects of debate. A ‘top down’ estimate of a bank is the cumulative difference of estimated production and the emission inferred from atmospheric observations using a model and a presumed lifetime. A ‘bottom-up’ bank estimates rely on a detailed analysis of applications that sequester the CFCs [McCullough *et al.*, 2001; McCullough *et al.*, 2003]. The top-down analysis was used by *Scientific Assessment of Ozone Depletion: 1998* [WMO, 1999] and *Scientific Assessment of Ozone Depletion: 2002* [WMO, 2003]. The bottom-up analysis is used by *Special Report: Safeguarding the ozone layer and the global climate system: Issues related to hydrofluorocarbons and perfluorocarbons* [IPCC, 2005]. Daniel *et al.* [2007] analyze the banks computed from a ‘top down’ analysis versus those computed from a bottom-up analysis. The maximum annual global emissions of chlorofluorocarbons (CFCs) took place during the late 1980s prior to the international agreements to ban production ( $\sim 350$  Ktons/year for  $\text{CFCl}_3$  and  $\sim 460$  Ktons/year for  $\text{CF}_2\text{Cl}_2$ ). These are far greater than estimates of emissions from banks, but the emissions from the banks are presently

comparable to annual atmospheric loss estimates and differences in the bank estimates are significant for decadal predictions. *Daniel et al. op cit.* point out that even small errors in lifetime accumulate, leading to uncertainty in the top-down bank estimates and also show that differences in bank estimates are large enough to impact predictions for future levels of CFCs and ozone recovery.

The purpose of this paper is to use a variety of model simulations to investigate the relationships among the atmospheric burden, the lifetime and the loss rates of CFCs. We present results from simulations that have both realistic and unrealistic distributions for the stratospheric age-of-air. We show that the lower stratospheric relationships between the fractional release of chlorine from  $\text{CFCl}_3$  and  $\text{CF}_2\text{Cl}_2$  and the age-of-air produced by simulations with realistic age-of-air match relationships derived from aircraft observations by *Schauffler et al.* [2003]. Models with faster circulations do not produce realistic age-of-air and also do not reproduce the observed relationship between fractional release and mean age. In all simulations the annual change in atmospheric burden is specified by the mixing ratio boundary conditions and is thus disconnected from the simulation loss. The fluxes are free to obtain any value as determined by interior transport and loss rates. In simulations with ‘young’ age-of-air the CFC lifetime is equal to or shorter than that presumed in WMO2007 and the inferred boundary flux of CFCs can be unrealistically large in the early part of the present century. In simulations with realistic age-of-air, the lifetime is longer than presumed in WMO2007 and the inferred boundary flux of CFCs is negative after about 2010. The negative flux is computed

because the annual decrease in atmospheric burden imposed by the boundary conditions exceeds the simulated loss.

The models used in this analysis are described in the following section. Simulation results are presented in section 3. In section 4 we build on the results of *Hall* [2000] and *Schoeberl et al.* [2000], using trajectory simulations of age spectra and annual stratospheric loss rates to explain the relationship between the mean age-of-air and the fractional release of CFCs. The implications of the comparisons with observations for determination of CFC lifetime and removal from the atmosphere are discussed in section 5. We also consider the possibility that a speed-up in the Brewer Dobson Circulation due to climate change will impact the annual CFC loss and thus the ozone recovery [e.g., *Butchart and Scaife*, 2001]. Conclusions follow in section 6.

## **2. Model Descriptions**

Two types of atmospheric numerical models are used to predict the response of ozone to changes in the composition and climate of the atmosphere. A chemistry/climate model (CCM) combines a representation of photochemical processes with a general circulation model (GCM). In a CCM, ozone and other radiatively active gases are transported by the simulation winds, and the computed constituent fields are used to compute net radiative heating rates for the GCM, ensuring consistency among dynamics, radiation and photochemistry. A chemistry transport model (CTM) differs from a CCM in that the meteorological information needed for constituent transport and to account for temperature dependence of photochemical processes is input to the model from an

external source such as a GCM or a data assimilation system. CTMs may be three-dimensional or two-dimensional (latitude/altitude) but heating rates that would be calculated from trace gas distributions in CTMs are not necessarily consistent with the input meteorological fields.

The surface boundary conditions for source gases including chlorofluorocarbons are specified for all simulations following scenario A1B of the *Scientific Assessment of Ozone Depletion: 2002* [WMO, 2002]. Scenario A1B was also used in the modeling studies presented in WMO2007. Another scenario, A1, presented in Table 8-5 of WMO2007 is virtually the same as scenario A1B up to 2010. Although there differences between scenarios A1B and A1 after 2010, these will not impact the results of this study. The models used for these multi-decadal simulations are described below; the simulations are summarized in Table 1.

We also use a trajectory approach described by *Schoeberl et al.* [2000] to produce age spectra and to interpret the relationship between the mean age of air and the constituent distributions. The trajectory model is summarized after descriptions of the CCM and the CTMs.

#### *The GEOS-4 CCM*

The Goddard CCM, described briefly by *Stolarski et al.* [2006a], combines the GEOS-4 GCM (Goddard Earth Observing System, Version 4, General Circulation Model) with a representation of stratospheric photochemistry. Here we refer to this model as CGCM.

158 *Pawson et al.* [2007] describe CGCM and its performance. The GCM dynamical core  
159 uses a flux form semi-Lagrangian transport scheme [*Lin and Rood*, 1996, 1997] and a  
160 quasi-Lagrangian vertical coordinate system [*Lin*, 1997] to ensure accurate representation  
161 of the transport by the resolved-scale flow. The *Lin and Rood* [1996] transport scheme is  
162 also used for constituent advection. The photochemical mechanism includes all  
163 photolytic, gas-phase and heterogeneous reactions thought to be of importance in the  
164 stratosphere. The photochemical scheme, an updated version of that used in the Goddard  
165 CTM [e.g., *Douglass and Kawa*, 1999 and references therein] uses family  
166 approximations and has been extensively tested through applications of the Goddard  
167 CTM [*Douglass et al.*, 2001; *Stolarski et al.* 2006b]. Reaction rate and cross section data  
168 are taken from the Jet Propulsion Laboratory Evaluation 14 [*Sander et al.*, 2003].  
169 Processes involving polar stratospheric clouds use the parameterization described by  
170 *Considine et al.* [2000]. In the troposphere ozone relaxes to the climatology described by  
171 *Logan* [1999]. The ozone simulated using the CTM with meteorological fields from the  
172 GCM was shown to compare well with the ozone climatology used in the GCM before  
173 attempting to couple the GCM and photochemistry. A clock tracer is included in the  
174 simulation, providing information about the three-dimensional distribution of the mean  
175 age of air but no information about the age spectrum. The spatial resolution for  
176 simulations presented here is 2° latitude by 2.5° longitude with 55 layers from the surface  
177 to 0.01 hPa. The Brewer Dobson circulation is shown to be realistic by comparisons with  
178 observations showing the rate of ascent of tropical moisture anomalies and the decrease  
179 of the amplitude of the anomalies with height [*Eyring et al.*, 2006]. A weakness of the  
180 CGCM, common among CCMs, is that its south polar vortex lasts several weeks longer

than is consistent with observations [Eyring *et al.*, 2006; Pawson *et al.*, 2007]. This deficiency will have minimal impact on the computed CFC lifetime. The CGCM simulations used in this work differ in duration, and source of sea surface temperatures (SST) and sea-ice distributions at the lower boundary. Past simulations (1950 – 2004 use the “HadISST” (Hadley Center Ice and Sea-Surface Temperature) data set of Rayner *et al.* [2003]. Future simulations are integrated until 2049 or later, and use output from coupled ocean-atmosphere model simulations: HadGem1 [Johns *et al.*, 2006] and NCAR CCSM3 [Kiehl *et al.*, 1998]. The CGCM simulations are summarized in Table 1. The CGCM simulations using the various SSTs are similar but not identical. Results shown below are from specific simulations, but the same conclusions are drawn from any of the simulations.

#### *Global Modeling Initiative CTM*

Strahan and Douglass [2004] and Douglass *et al.* [2004] describe and evaluate the GMI CTM and the simulations used here. This version of the GMI CTM uses the same advection scheme, the same look-up tables for the photolysis calculation and essentially the same photochemical mechanism as the CGCM described above. Horizontal resolution for these simulations is 4° latitude x 5° longitude, with 28 vertical levels from the surface to 0.4 hPa. Individual species are advected separately with the exception of some radical species, and the photochemical contribution to the individual tendency equations are calculated using SMVGEAR II [Jacobson, 1998]. Experiments in which a ‘pulse’ of a conserved tracer is emitted and tracked provide information about the annual mean age of air and the age spectrum. The two simulations differ only in the input meteorological fields. One set of meteorological fields is taken from a GCM that uses a

version of the GEOS-4 GCM dynamical core described above and was developed through a collaboration of NASA with the National Center for Atmospheric Research. The second set of fields is taken from a version of the Goddard Earth Observing System Data Assimilation System (GEOS-DAS). This version of GEOS-DAS uses this same GCM in the assimilation process. *Strahan and Douglass* [2004] and *Douglass et al.* [2004] provide many details about the input meteorological fields and extensive comparisons with observations. The comparisons show that the short-lived radicals such as ClO and NO<sub>2</sub> and longer-lived reservoir species such as HCl, ClONO<sub>2</sub> and HNO<sub>3</sub> compare well with observations. However, the overturning circulation associated with this version of GEOS-DAS is much more rapid than that produced by the GCM, and comparisons involving long-lived source gases show that transport produced by the GCM fields is more realistic than that produced using the assimilated meteorology [*Douglass et al.*, 2003]. In the remainder of this paper, simulations using the GMI CTM with meteorological fields from the GCM and GEOS-DAS are referred to as GMI-GCM and GMI-DAS respectively.

#### *Two-Dimensional CTM*

The GSFC two-dimensional (2D) CTM, originally discussed in *Douglass et al.* [1989] and *Jackman et al.* [1990], has undergone steady upgrades and improvements [*Fleming et al.*, 2007 and references therein]. The present version uses changing transport fields over the 1958-2004 period and a climatology for years 2005-2050, all from the National Centers for Environmental Prediction- National Center for Atmospheric Research reanalysis project. *Fleming et al.* [2007] show that long-lived tracers produced using

these transport fields compare well with observations. Here the 2D CTM vertical domain extends from the ground to approximately 92 km with levels separated by ~2 km. The horizontal domain extends from pole to pole, with 18 boxes of 10 degrees latitude. The photochemical mechanism includes largely the same reactions as used in the 3D models described above, and also uses kinetic information from the Jet Propulsion Laboratory Evaluation 14 [Sander *et al.*, 2003]. Simulations using this most recent updated version of the 2D CTM are referred to here as 2D-base.

An earlier version of the 2D CTM, the “1995 model” described in Fleming *et al.* [1999, 2001] produces much shorter age-of-air than indicated by measurements. This version of the 2D CTM is referred to as 2D-fast and provides a contrast to the more realistic 2D-base version.

Table 1: A summary of the simulations used in this work. SST1= observed (Hadley); SST2= Modeled HadGEM1; SST3=Modeled NCAR CCM3

model	duration	Realistic Age of air
2D-base	1935 - 2099	yes
2D-fast	1935 - 2099	no
GMI-GCM	1995 - 2030	yes
GMI-DAS	1995 - 2030	no
CGCM		
P1 SST1	1950 – 2004	yes
P2 SST1	1950 – 2004	yes

F1 SST2	1996 – 2099	yes
F2 SST2	1971 – 2049	yes
F3 SST3	1971 – 2052	yes
F4 SST3	2000 – 2099	yes

243

### 244 *Trajectory Model*

245 *Schoeberl et al.* [2000, hereafter S2000] describe the 2D trajectory model in detail. The  
 246 trajectory model uses the residual circulation and mixing coefficients of the 2D CTM.  
 247 The residual circulation is computed from diabatic heating rates, and the trajectory model  
 248 scrambles vertical and horizontal positions to simulate mixing [*Feller*, 1968]. S2000  
 249 show that the parcel spectra produced by long simulations using a 3D trajectory model  
 250 are similar to those produced by this 2D model. The 2D trajectory model is used because  
 251 it is more than 100 times faster than an equivalent 3D calculation.

252

## 253 **3. Simulation Results**

254 Simulated fields for the present and near past can be compared with data from various  
 255 sources to evaluate the representation of the atmosphere by the model. Here we make  
 256 some comparisons with observations in order to assess the potential uncertainties in any  
 257 projections into the future and contrast results from different simulations.

258

### 259 *Loss Rate Distributions*

260 The annual average local lifetimes (inverse of the local chemical loss frequency) for  
 261  $\text{CFCl}_3$  and  $\text{CF}_2\text{Cl}_2$  are shown in Figure 1. The shading emphasizes the narrow transition

separating a region with a lifetime of two years or longer from a region with lifetimes of a few months or less. For  $\text{CFCl}_3$  ( $\text{CF}_2\text{Cl}_2$ ) parcels below 50 hPa (20 hPa) outside the tropics have local lifetimes of two years or longer. Air parcels that remain below the shaded transition region retain most of their  $\text{CFCl}_3$  ( $\text{CF}_2\text{Cl}_2$ ) while those that go above the transition have their  $\text{CFCl}_3$  ( $\text{CF}_2\text{Cl}_2$ ) rapidly converted to  $\text{Cly}$ .

We compare results from the five simulations with the models described in Section 2 to demonstrate the relationship of the circulation to the loss rates and time-evolving burden of chlorofluorocarbons. The annual-averaged loss distributions ( $\# \text{ cm}^{-3} \text{ s}^{-1}$ ) for each of the simulations are shown for  $\text{CFCl}_3$  and  $\text{CF}_2\text{Cl}_2$  for the year 2000 in Figure 2. For  $\text{CFCl}_3$  most of the loss takes place in the tropics below 10 hPa. There is no significant loss above 10 hPa because destruction below is sufficiently rapid that  $\text{CFCl}_3$  is destroyed before parcels reach that level. Parcels between 10 and 30 hPa at middle latitudes are similarly depleted of  $\text{CFCl}_3$  so there is little loss in spite of short chemical lifetimes. Parcels in the lower stratosphere middle latitudes contribute little to the loss because the destruction rate is slow. A similar discussion applies to the loss distributions for  $\text{CF}_2\text{Cl}_2$ , but the region of the greatest loss is found at a higher altitude as expected from the difference in lifetimes (Figure 1).

It is clear from Figure 2 that the simulations with faster circulations (GMI-DAS and 2D-fast) have larger total loss rates than the CGCM, GMI-GCM and 2D-base. Stronger upwelling shifts the tropical constituent profiles upward and the loss, the product of the mixing ratio and the destruction rate, is commensurately greater.

## *Age of Air and Cly Distributions*

Circulation differences among the models are also apparent through comparison of the stratospheric age-of-air derived from the simulations. These differences can be evaluated by comparison to observations [Boering *et al.*, 1996] as in Figure 3. The values produced by the CGCM, 2D-base and GMI-GCM fall within the  $2\sigma$  limits of values derived from observations poleward of about  $15^\circ$  latitude. There is a small offset in the tropics. The 2D-fast and GMI-DAS simulations both produce age distributions that are young compared with the values derived from observations, and could both be described as having fast circulations. The other three could be said to have realistic (slow) circulations.

An important test of the circulation and its interaction with photochemical destruction is provided by the fractional release of chlorine from CFCs. In the upper stratosphere,  $\text{CFCl}_3$  and  $\text{CF}_2\text{Cl}_2$  are nearly completely photolyzed in all simulations, and  $\text{Cl}_y$  time series from different simulations are nearly identical, as shown by time series for GMI-GCM and GMI-DAS at  $2^\circ\text{N}$  and 1.3 hPa in Figure 4(a). The  $\text{Cl}_y$  distributions are quite different in the two simulations below 10 hPa with significantly higher values of  $\text{Cl}_y$  in GMI-GCM compared with GMI-DAS as shown for annually averaged  $\text{Cl}_y$  in Figure 4(b). The differences are greater than 10 percent for most of the region between 70 and 10 hPa, and are greater than 30% in much of the southern hemisphere (Figure 4(c)). We test the realism of the ‘fast’ versus the ‘slow’ circulation using aircraft observations of  $\text{CFCl}_3$  and  $\text{CF}_2\text{Cl}_2$

308 *Fractional Release*

309 *Schauffler et al.* [2003] use aircraft observations of various long-lived source gases to  
310 compute the fractional release (fr)

311 
$$fr = (1 - \chi(\mathbf{x})/\chi_i)$$

312 where  $\chi(\mathbf{x})$  is the mixing ratio of a chlorofluorocarbon in a parcel at location  $\mathbf{x}$  (latitude,  
313 altitude, pressure, time) and  $\chi_i$  is the mixing ratio that the parcel would have had no loss  
314 occurred. We estimate  $\chi_i$  using the mean age to determine the constituent mixing ratio at  
315 the time of entry at the tropical tropopause (i.e., the time of the measurement of  $\chi$  minus  
316 the mean age). We tested this approximation by comparing the mean of the distribution  
317 of initial mixing ratios calculated from the constituent time series at the tropical  
318 tropopause using the GMI age spectra calculated with  $\chi_i$  calculated using the mean age.  
319 The age spectra are not symmetric and have a tail of elements corresponding to older ages.  
320 Each element  $j$  is associated with a different entry value  $\chi_i^j$  because the CFCs are  
321 increasing with time. The means of the initial values associated with each element in the  
322 age spectrum are only a few percent smaller than values  $\chi_i$  calculated using the mean age.

323

324 *Schauffler et al.* [2003] find a compact relationship between mean age of air and the  
325 fractional release in the lower stratosphere using observations from several aircraft  
326 campaigns. The simulations considered here produce compact relationships for  $\text{CFCl}_3$   
327 and  $\text{CF}_2\text{Cl}_2$  at  $\sim 50$  hPa (a comparable height to the observations). These are shown in  
328 Figure 5 along with the fractional releases and mean ages derived from observations by

*Schauffler et al.* [2003]. For observations and for all simulations, fractional release increases monotonically with age. Simulations using the slower circulations (CGCM, GMI-GCM and 2D-Base), with realistic values for mean age-of air (Figure 3), produce relationships between mean age and fractional release similar to those derived from observations. The fractional releases of both compounds are somewhat larger than observed for air masses with older mean age, with larger differences for  $\text{CF}_2\text{Cl}_2$ . The fast circulations (GMI-DAS and 2D-fast) produce relationships that are clearly separated from those derived from observations or produced by the other simulations (Figure 5).

The ranges of values are somewhat smaller for the GMI simulations than for any of the other simulations. The annual zonal mean age is determined for both GMI simulations using “pulse” experiments; this is plotted vs. the fractional release calculated from annual zonal mean tracer fields. The mean age for CGCM is calculated using a “clock” tracer, and its seasonal and longitudinal variations are matched with similar variations in tracer fields. The ranges of age and fractional release using annually zonal averaged fields are reduced by the temporal and spatial averaging but the relationship between them is similar to that obtained with the other simulations.

#### *Budgets for $\text{CFCl}_3$ and $\text{CF}_2\text{Cl}_2$*

The rate of change of a particular CFC’s burden  $B$  satisfies a conservation equation

$$\partial B / \partial t = F - B / \tau \quad (1)$$

where  $F$  is the flux (i.e., the emissions into the atmosphere) and  $\tau$  is the atmospheric lifetime of that CFC. In all of our simulations, the CFC mixing ratio in the boundary layer

is specified. Because the mass of the stratosphere is small and the entire troposphere responds to the boundary conditions, the total atmospheric burdens of  $\text{CFCl}_3$  or  $\text{CF}_2\text{Cl}_2$  and the year-to-year changes in the atmospheric burden are largely governed by the boundary conditions. The annual-average atmospheric losses ( $B/\tau$ ) for  $\text{CFCl}_3$  and  $\text{CF}_2\text{Cl}_2$  as functions of time for the recent past and the future are compared in Figure 6 for each of the five simulations. Between 2000 and 2030 the integrated loss is much higher for the two simulations with fast circulations. The simulations with different losses maintain balance between the annual change in burden ( $\partial B/\partial t$ ), the annual loss terms  $B/\tau$  and the input to the atmosphere with different implied fluxes of  $\text{CFCl}_3$  and  $\text{CF}_2\text{Cl}_2$  at the lower boundary. Equation 1 can be solved for the flux necessary to produce the change in burden that is imposed by the mixing ratio boundary conditions. The net atmospheric losses up until 2002 for  $\text{CF}_2\text{Cl}_2$  and  $\text{CFCl}_3$  from CGCM, 2D-base and 2D-fast (the three simulations that span the appropriate temporal domain) are compared in Table 2. The differences among the simulations are not large compared with the estimated total input to the atmosphere as shown by the last column which is the maximum difference divided by the estimated total atmospheric input.

Table 2. Net atmospheric losses up until 2002 (in kilotons).

	CGCM	2D-base	2D-fast	$\Delta\text{loss}/(\text{total input})$
$\text{CFCl}_3$	2310	2630	3200	0.10
$\text{CF}_2\text{Cl}_2$	2340	2480	2730	0.03

370 The fluxes inferred from the burden change and simulation losses for the 2D-base and 2D-  
371 fast simulations are compared with industrial estimates in Figure 7a for  $\text{CFCl}_3$  and Figure  
372 7b for  $\text{CF}_2\text{Cl}_2$ . Fluxes were not shown for the GMI simulations as they begin in 1995  
373 when emissions to the atmosphere have already declined substantially from their late  
374 1980's maxima. The CGCM simulations are not shown because they used the mixing  
375 ratios recorded on the CCMVal website at 5-year intervals with a linear interpolation  
376 between. This does not alter any of the results presented here, but the deduced flux has  
377 unrealistic jumps at 5- year intervals.

378

379 Up until about 1980 the emissions of CFCs increase rapidly and the change in burden  
380 ( $\partial B/\partial t$ ) is significantly larger than the photochemical loss for a given year ( $\partial B/\partial t \gg B/\tau$ ,  
381 so  $\partial B/\partial t \approx F$ ), thus differences in the simulated loss rates lead to very small differences in  
382 the deduced flux. In later years, as  $\partial B/\partial t$  decreases, the model differences in the total loss  
383 rates leads to a substantial difference in the fluxes deduced for the fast and realistic  
384 simulations. The  $\text{CFCl}_3$  flux computed with 2D base is consistently smaller than the  
385 bottom-up estimate of emissions [McCullough *et al.*, 2001]. The 2D base  $\text{CF}_2\text{Cl}_2$  flux is  
386 also smaller than the bottom-up estimate [McCullough *et al.*, 2003], but the discrepancy  
387 is smaller. We infer from differences in the losses in Figure 6 that the CGCM flux for  
388  $\text{CF}_2\text{Cl}_2$  would be closer to the data while that for  $\text{CFCl}_3$  would be in worse agreement.  
389 This inconsistency for  $\text{CFCl}_3$  but not for  $\text{CF}_2\text{Cl}_2$  is similar to results obtained by Gupta *et*  
390 *al.* [2001], who compare computed surface mixing ratios with observations and conclude

that the  $\text{CFCl}_3$  emissions are too large. The CFC lifetimes produced by the model used by *Gupta et al.* [2001] are similar to those produced by the CGCM.

The differences in the losses are also significant in the later years, after  $\sim 2020$ , when the input of CFCs to the atmosphere is expected to be negligible (i.e.,  $F \approx 0$ ). We compare the fluxes inferred from the burden change and the simulated losses for 2000-2050 in the bottom panels of Figure 8. The GMI-DAS circulation has by far the greatest annual loss of  $\text{CFCl}_3$  and  $\text{CF}_2\text{Cl}_2$  (light blue dashed-dotted line in Figure 6) and the inferred fluxes are much greater than the expected zero value. For the three simulations with realistic age of air (CGCM, GMI-GCM and 2D-base) the simulated loss of  $\text{CFCl}_3$  is less than that required for consistency with the annual change in atmospheric burden, so the inferred fluxes are negative. Negative flux means that the  $\text{CFCl}_3$  is being removed from the atmosphere by processes other than the stratospheric losses, i.e., the mixing ratio boundary condition creates an artificial surface loss. For the CGCM simulations the negative flux of  $\text{CFCl}_3$  is about 20% of stratospheric loss after 2020. If we implemented flux boundary conditions in the CGCM, the burden of  $\text{CFCl}_3$  would decline more slowly than presently forecast.

The annual change in burden is generally better matched by the computed losses for  $\text{CF}_2\text{Cl}_2$ . As for  $\text{CFCl}_3$ , GMI-DAS requires a significant positive flux to maintain consistency with the  $\text{CF}_2\text{Cl}_2$  burden. A small positive flux is calculated for 2D-fast. The

magnitudes of the inferred fluxes calculated for the CGCM (2 cases), GMI-GCM and 2D-base are within 5% of the annual loss.

We compare the lifetimes ( $\tau$  = model loss/model burden) that are internally calculated for the two CGCM simulations, GMI-GCM, 2D-base, GMI-DAS and 2D-fast in the top two panels of Figure 8. The  $\text{CFCl}_3$  lifetimes  $\sim 2005$  are substantially longer than the 45 year lifetime used in recent WMO assessments to produce the mixing ratio scenarios used by CGCM, GMI-GCM and 2D-base. The lifetime range for the models with realistic age-of-air, 56-64 years, is inconsistent with both the  $\text{CFCl}_3$  lifetime used in the WMO assessments and outside the observationally derived range of  $41 \pm 12$  years reported by *Volk et al.* [1997]; the quoted uncertainty of 12 years is one-sigma. The 2D-fast lifetime is the same value as used in assessments; the GMI-DAS lifetime is smaller but within the range derived by *Volk et al.* [1997]. The  $\text{CF}_2\text{Cl}_2$  lifetime for GMI-DAS (80 years) is close to the middle of the range derived by *Volk et al.* [1997], and is shorter than the lifetime used in assessments (100 years). The other simulations produce  $\text{CF}_2\text{Cl}_2$  lifetimes within 10% of the lifetime used in the assessments.

The lifetimes in the CGCM simulations decrease with time throughout the integration because the overturning circulation speeds up, a common feature of this sort of model [*Butchart et al.*, 2006]. This will be discussed in Section 6.

#### 4. The relationship between mean age-of-air and fractional release

In order to understand the relationship between the mean age-of-air and the fractional release (Figure 5), we have calculated age spectra using the 2D trajectory model following the approach of S2000. Five-year back trajectory histories are calculated for 2000 parcels originally located within  $0.5^\circ$  latitude and 0.25 km of 55N, 21 km. This location is chosen to illustrate the relationships; other locations in the lower stratosphere extra-tropics behave similarly. To avoid confusion we refer to each parcel as an element of the age spectrum. The age spectrum produced by this calculation is shown in Figure 9(a). The time when the each element crosses the tropical tropopause is its age – fewer than 1% of the 2000 parcels fail to cross the tropical tropopause during the integration. These elements are assigned an age of 5 years. The old age tail is obviously truncated by this approach, but resolving the tail would require thousands of elements and a much longer period of integration without impacting the results as will be clear from the discussion below.

The fractional releases of  $\text{CFCl}_3$  and  $\text{CF}_2\text{Cl}_2$  are calculated for each element using an annual mean loss rate. For each element an entry value for each CFC mixing ratio is calculated at the tropical tropopause using the time series of tropospheric mixing ratios and the age of the element. The amount of CFC remaining in each element is calculated by integrating forward from the tropical tropopause along the trajectories, interpolating the annual mean loss to the location of the element at each time step. The distributions of fractional release are given in Figure 9(b) for  $\text{CFCl}_3$  and 9(c) for  $\text{CF}_2\text{Cl}_2$ . The fraction of elements is shown on a log scale for  $\text{CFCl}_3$  and  $\text{CF}_2\text{Cl}_2$  to show that there are a few

elements that have lost most of their  $\text{CF}_2\text{Cl}_2$ . About 12% of the 2000 elements have lost more than 90% of their  $\text{CFCl}_3$ ; only 1% of the elements have lost a comparable fraction of  $\text{CF}_2\text{Cl}_2$ .

The relationship between the fractional release and the age spectrum is not obvious from the distributions shown in Figure 9. The relationship is clarified somewhat by plotting the fractional releases and the maximum altitudes experienced along the trajectories as functions of the age of the elements as shown in Figure 10.

For  $\text{CFCl}_3$  (Figure 10a) the relationship between the age of the element and fractional release is fairly compact and linear for ages less than 1.5 years; 35% of the elements fall in this range. For older ages a much wider range of fractional releases is possible; for ages greater than 3 years 10% of the elements have fractional releases of 0.95 or greater.

The maximum loss of  $\text{CF}_2\text{Cl}_2$  takes place at higher altitude (Figure 2), and this is reflected by Figure 10b. The relationship between fractional release and age is fairly compact and linear for element ages less than 2.5 – 3 years, but there is little correlation between the fractional release and element age for older ages. The relationship between the age of the element and the maximum altitude is also much more compact for elements younger than three years (Figure 10c). This result is consistent with the findings of *Hall* [2000] who also studied the maximum altitude distribution of elements of the age spectrum.

S2000 present a conceptual framework for the relationship between the mean age and the tracer amount for long-lived tracers and show that under an average path approximation

the tracer amount is more strongly related to the age than to the parcel path. The results of Figure 10 support the relationship between tracer amount and age for younger elements in the age spectrum but behavior is different for the older elements. We explore this result further by plotting the fractional release as a function of the maximum altitude experienced by the element (Figure 11). There is a compact relationship between the fractional release for each element and its maximum altitude for both CFCs. Elements with maximum altitudes greater than 30 km experience virtually complete loss of  $\text{CFCl}_3$  and are insensitive to further increases in maximum altitude. For  $\text{CF}_2\text{Cl}_2$  the fractional release increases with increasing maximum altitude.

To clarify the relationship between the age of the elements and the maximum height, we bin the elements according to their ages (0-1 yr, 1-2 yr, etc.) and compute the mean and standard deviation of the age and the associated maximum heights. These are shown in Figure 12. Elements associated with older age intervals experience a much broader range of maximum heights than those with younger ones as was found by *Hall* [2000]. Also note that elements with ages younger than 3 years have fractional release values for  $\text{CF}_2\text{Cl}_2$  less than 0.2 (Figure 10(b)), consistent with the result that the elements rarely if ever rise above 30 km and thus do not experience rapid destruction of  $\text{CF}_2\text{Cl}_2$ . This analysis shows that a significant fraction of the air in the lower stratosphere with mean age greater than a few years and fractional releases of  $\text{CF}_2\text{Cl}_2$  greater than 0.4 as reported by *Schauffler et al.* [2003] has at some time experienced heights above 30 km.

The simulated fractional release values for  $\text{CF}_2\text{Cl}_2$  and  $\text{CFCl}_3$  from the two simulations with fast circulations (GMI-DAS and 2D-fast) are greater for younger ages than those

calculated with the slower circulations. These values are also greater than observed. This result makes sense in the context of the trajectory calculations. The elements in the age spectra for the faster circulations must be associated with higher maximum altitudes than elements with similar ages from the age spectra for the slower circulations, thus more chlorine is released from the CFCs in these circulations even though their residence time in the stratosphere is reduced due to the more rapidly overturning circulation.

## 5. Future age and fractional release distributions

As noted above, the lifetimes of  $\text{CFCl}_3$  and  $\text{CF}_2\text{Cl}_2$  calculated for CGCM simulations decrease as the integrations progress (Figure 8). *Austin and Li* [2006] show that the mean age decreases as the strength of the overturning circulation increases using a similar CCM. The CGCM mean age decreases globally throughout the simulation; the difference in the zonal mean age between 1995 and 2045 is shown in Figure 13 for one simulation; all simulations show similar patterns. In the lower stratosphere the fractional release and mean age exhibit a compact relationship (Figure 5). The compact relationships change with time because the mean age is more sensitive to the simulated change in circulation than the fractional release (Figure 14). The mean age decreases everywhere in the stratosphere (Figure 13), but the fractional release can decrease, remain nearly constant, or can increase. We emphasize this point by computing the change in fractional release five year means centered on 2002 and 2047 in two ways. The changes for  $\text{CFCl}_3$  and  $\text{CF}_2\text{Cl}_2$  are given in Figure 15(a) and 15(b). Figures 15(c) and 15(d) show the change for the same time period that would be obtained assuming a fixed relationship between

fractional release and mean age. Note that the changes are much larger for 15(c) and 15(d), and the scales also differ. Similar patterns are obtained for all simulations.

As shown in Figure 13, the mean age is younger throughout the stratosphere; the largest changes are found at middle and high latitudes in the lower stratosphere. The patterns of change in fractional releases for  $\text{CFCl}_3$  and  $\text{CF}_2\text{Cl}_2$  are consistent with the change in the circulation. In the tropics parcels are transported upward more rapidly. Tracer profiles are displaced upward slightly leading to increased loss, but the fractional releases decrease due to a shorter residence time. The largest decrease in the fractional release of  $\text{CFCl}_3$  is seen in the region of maximum loss, i.e., between 50 and 30 hPa (Figure 2 and Figure 15a). For  $\text{CF}_2\text{Cl}_2$  the largest decrease in fractional release is between 20 and 5 hPa (Figure 2 and Figure 15b). Outside the tropics the fractional release changes very little as the mean age decreases, suggesting that although some elements in the age spectrum experience higher maximum heights and greater loss, this is balanced by the overall shift in the age spectrum towards younger ages. The shift in the relationship between the mean age and the fractional release as the circulation speeds up is explained by the relationships between the age spectrum, the maximum height, and the fractional release explored in the previous section. Figures 15c and 15d assume that the relationships between the fractional releases and the mean ages are unchanged, and show a completely different pattern from that produced by the CGCM simulations. Under this assumption, the fractional release would always decrease as the age decreases. The largest changes would occur in the

middle high latitude lower stratosphere, the opposite of what is produced by the simulations.

## **6. Discussion and Conclusions**

In all current ozone assessment, ODS mixing ratios are specified as model boundary conditions. The use of these mixing ratio boundary conditions for the past record guarantees that the tropospheric mixing ratios match observations. Even so, the amount of inorganic chlorine in the atmosphere varies significantly among simulations because the loss rates of the chlorofluorocarbons vary for different circulations.

The modeled mixing ratios of  $\text{Cl}_y$  and HCl in the upper atmosphere are largely controlled by the mixing ratio boundary conditions; the exact timing of the maxima will vary if the times to propagate the boundary conditions to the upper atmosphere differ. The amount of  $\text{Cl}_y$  in the lower stratosphere is strongly influenced by differences in circulation among various simulations. If flux boundary conditions were used the level of  $\text{Cl}_y$  in the upper stratosphere and its rate of increase and decline would also vary depending on the simulation circulation and transport through their impact on the loss rate, and comparisons with time series would provide additional information about model performance. For example, *Lary et al.* [2007] have combined measurements of various chlorine species to produce a global estimate of  $\text{Cl}_y$  for 1991-2006. *Froidevaux et al.* [2006] demonstrate that upper stratospheric chlorine decreased between July 2004 and December 2005.

570

571 The question of the amount of chlorofluorocarbons that is presently ‘banked’ and the rate  
572 of release to the atmosphere is difficult to address. Top-down and bottom-up estimates  
573 differ, thus the projections for future atmospheric levels of CFCs are uncertain. We find  
574 that the magnitude of the fluxes needed to maintain the mixing ratio boundary conditions  
575 in our simulations depends on the overall vigor of the atmospheric circulation.  
576 Comparisons with observations presented by *Pawson et al.* [2007] as well as the  
577 comparisons with age-of-air and fractional release shown here indicate that the  
578 circulations and destruction rates of CGCM, GMI-GCM and 2D-base are more realistic  
579 than those of GMI-DAS and 2D-fast. An important implication of these results is that  
580 simulations with realistic age-of-air and fractional release of chlorine yield longer  
581 atmospheric lifetimes for chlorofluorocarbons. The effect is greater for  $\text{CFCl}_3$  (56 years  
582 vs 45 years) than for  $\text{CF}_2\text{Cl}_2$  (101-110 years vs 100 years). The difference in the loss  
583 estimates is comparable to the difference in the bank estimates for the ‘bottom up’ and  
584 ‘top down’ evaluations reported by *Daniel et al.* [2007]. If these longer lifetimes are  
585 more appropriate, the amounts of  $\text{CFCl}_3$  and  $\text{CF}_2\text{Cl}_2$  stored in banks estimated from  
586 bottom-up calculations would increase and agree better with the top-down estimates.  
587 Finally, we find that the lifetime decreases as the circulation speeds up due to climate  
588 change as in most CCM calculations. Flux boundary conditions for long-lived gases must  
589 be used to test whether the change in the loss due to the circulation speed-up has a  
590 significant impact on the decline of CFCs in the atmosphere.

591

## References

- Austin, J. and F. Li (2006), On the relationship between the strength of the Brewer-Dobson circulation and the age of stratospheric air, *Geophys. Res. Lett.*, *33*, doi:10.1029/2006GL026867.
- Boering, K. A., S. C. Wofsy, B. C. Daube, H. R. Schneider, M. Loewenstein, and J. R. Podolske (1996), Stratospheric mean ages and transport rates from observations of carbon dioxide and nitrous oxide, *Science*, *274*(5291), 1340–1343.
- Butchart, N., and A. A. Scaife (2001), Removal of chlorofluorocarbons by increased mass exchange between the stratosphere and troposphere in a changing climate, *Nature*, *410*, 799-802.
- Butchart et al. (2006), Simulations of the anthropogenic change in the strength of the Brewer-Dobson circulation, *Clim. Dyn.*, *27*, 727-741.
- Considine, D. B., A. R. Douglass, P. S. Connell, D. E. Kinnison, and D. A. Rotman, (2000), A polar stratospheric cloud parameterization for the global modeling initiative three-dimensional model and its response to stratospheric aircraft, *J. Geophys. Res.*, *105*, 3955-3973.
- Daniel J. S., G. J. M. Velders, S. Solomon, M. McFarland, S. A. Montzka (2007), Present and future sources and emissions of halocarbons: Toward new constraints, *J. Geophys. Res.*, *112*, D02301, doi:10.1029/2006JD007275.
- Douglass, A. R., C. H. Jackman, and R. S. Stolarski (1989), Comparison of model results transporting the odd nitrogen family with results transporting separate odd nitrogen species, *J. Geophys. Res.*, *94*, 9862-9872.

614 Douglass, A. R. and S. R. Kawa (1999), Contrast between 1992 and 1997 high-latitude  
 615 spring Halogen Occultation Experiment observations of lower stratospheric HCl,  
 616 *J. Geophys. Res.*, *104*, 18,739-18,754.

617 Douglass, A. R., M. R. Schoeberl, S. R. Kawa and E. V. Browell (2001), A composite  
 618 view of ozone evolution in the 1995-1996 northern winter polar vortex developed  
 619 from airborne lidar and satellite observations, *J. Geophys. Res.*, *106*, 9879-9895.

620 Douglass, A. R., M.R. Schoeberl, R. B. Rood and S. Pawson (2003), Evaluation of  
 621 transport in the lower tropical stratosphere in a global chemistry and transport  
 622 model, *J. Geophys. Res.*, *108*, 4259, 2002JD002696.

623 Douglass, A. R., R. S. Stolarski, S. E. Strahan, P. S. Connell (2004), Radicals and  
 624 reservoirs in the GMI chemistry and transport model: Comparison to  
 625 measurements, *J. Geophys. Res.*, *109*, D16302, doi:10.1029/2004JD004632.

626 Eyring V., et al. (2006), Assessment of temperature, trace species, and ozone in  
 627 chemistry-climate model simulations of the recent past, *J. Geophys. Res.*, *111*,  
 628 D22308, doi:10.1029/2006JD007327.

629 Feller, W., An Introduction to Probability Theory and Its Applications, vol. 1, John Wiley  
 630 New York, 1968.

631 Fleming, E. L., C. H. Jackman, R. S. Stolarski, and D. B. Considine (1999), Simulation of  
 632 stratospheric tracers using an improved empirically based two-dimensional model  
 633 transport formulation, *J. Geophys. Res.*, *104*, 23911-23934.

634 Fleming, E. L., C. H. Jackman, D. B. Considine, and R. S. Stolarski (2001), Sensitivity of  
 635 tracers and a stratospheric aircraft perturbation to two-dimensional model  
 636 transport variations, *J. Geophys. Res.*, *106*, 14245-14263.

637 Fleming, E. L., C. H. Jackman, D. K. Weisenstein, and M. K. W. Ko (2007), The impact  
638 of interannual variability on multi-decadal total ozone simulations, *J. Geophys.*  
639 *Res.*, *112*, D10310, doi:10.1029/2006JD007953.

640 Froidevaux L. et al. (2006), Temporal decrease in upper atmospheric chlorine, *Geophys.*  
641 *Res. Lett.*, *33*, L23812, doi:10.1029/2006HL027600.

642 Gupta, M. L., R. P. Turco, C. R. Mechoso and J. A. Spahr, On-line simulations of passive  
643 chemical tracers in the University of California, Los Angeles, atmospheric general  
644 circulation model 1. CFC-11 and CFC-12 (2001), *J. Geophys. Res.*, *106*, 12401-  
645 12417.

646 Hall, T. M. (2000), Path histories and timescales in stratospheric transport: Analysis of an  
647 idealized model, *J. Geophys. Res.*, *105*, 22811-22823.

648 Intergovernmental Panel on Climate Change/Technology and Economic Assessment  
649 Panel (2005), IPCC Special Report: Safeguarding the Ozone Layer and the Global  
650 Climate System: Issues Related to Hydrofluorocarbons and Perfluorocarbons, 478  
651 pp., Cambridge Univ. Press, New York.

652 Jackman, C. H., A. R. Douglass, R. B. Rood, R. D. McPeters, and P. E. Meade (1990),  
653 Effect of solar proton events on the middle atmosphere during the past two solar  
654 cycles as computed using a two-dimensional model, *J. Geophys. Res.*, *95*, 7417-  
655 7428.

656 Jacobson, M. Z. (1998), Improvement of SMVGEAR II on vector and scalar machines  
657 through absolute error tolerance control, *Atmos. Environ.*, *32*, 791-796.

658 Johns, T.C., et al. (2006), “The new Hadley Centre Climate Model (HadGEM1):  
659 Evaluation of coupled simulations”, *J. Climate* *19*, 1327-1353.

660 Kiehl, J.T., J.J. Hack, G.B. Bonan, B.A. Boville, D.L. Williamson, and P.J. Rasch (1998),  
661 "The National Center for Atmospheric Research Community Climate Model:  
662 CCM3" *J. Climate* 11, 1131-1149.

663 Lary D.J., D. W. Waugh, A. R. Douglass, R. S. Stolarski, P. A. Newman, H. Mussa  
664 (2007), Variations in stratospheric inorganic chlorine between 1991 and 2006,  
665 *Geophys. Res. Lett.* in press.

666 Lin, S.-J. and R. B. Rood, Multidimensional flux form semi-Lagrangian transport  
667 schemes, *Mon. Wea. Rev.*, 124, 2040-2070, 1996.

668 Lin, S.-J., A finite-volume integration scheme for computing pressure-gradient forces in  
669 general vertical coordinates, *Q. J. R. Meteorol. Soc.*, 123, 1749-1762, 1997.

670 Lin, S.-J. and R. B. Rood, An explicit flux-form semi-Larangian shallow water model on  
671 the sphere, *Q. J. R. Meteorol. Soc.*, 123, 2477-48, 1997.

672 Logan, J. A. (1999), An analysis of ozonesonde data for the troposphere:  
673 Recommendations for testing 3-D models and development of a gridded  
674 climatology for tropospheric ozone, *J. Geophys. Res.*, 104, 16,115-16,150.

675 McCulloch, A., P. Ashford, P. M. Midgley (2001), Historic emissions of  
676 fluortrichloromethane (CFC-111) based on a market survey, *Atmospheric*  
677 *Environment* 35, 4387-4397.

678 McCulloch, A., P. M. Midgley, P. Ashford (2003), Releases of refrigerant gases (CFC-  
679 12, HCFC-22 and HFC-134a) to the atmosphere, *Atmospheric Environment* 37,  
680 889-902.

681 Newman, P. A., E. R. Nash, S. R. Kawa, S. A. Montzka and S. M. Schauffler (2006),  
 682 When will the Antarctic ozone hole recover, *Geophys. Res. Lett.*, 33, L12814,  
 683 doi:10.1029/2005GL025232.

684 Pawson, S., R. S. Stolarski, A. R. Douglass, P. A. Newman, J. Nielsen, Mohan L.  
 685 Gupta (2007), Goddard Earth Observing System chemistry-climate model  
 686 simulations of stratospheric ozone-temperature coupling between 1950 and 2005,  
 687 submitted to *J. Geophys. Res.*

688 Rayner, N. A., D. E. Parker, E. B. Horton, C. K. Folland, L. V. Alexander, D. P. Rowell,  
 689 E. C. Kent and A. Kaplan, Global analyses of sea surface temperature, sea ice and  
 690 night marine air temperature since the late nineteenth century (2003), *J. Geophys.*  
 691 *Res.*, 108, 4407.

692 Sander, S. P., et al. (2003), Chemical kinetics and photochemical data for use in  
 693 atmospheric studies, Evaluation number 14, JPL Publ. 02-25.

694 Schauffler, S. M., E. L. Atlas, S. G. Donnelly, A. Andrews, S. A. Montzka, J. W. Elkins,  
 695 D. F. Hurst, P. A. Romashkin, G. S. Dutton and V. Stroud, Chlorine budget and  
 696 partitioning during the Stratospheric Aerosol and Gas Experiment (SAGE) III  
 697 Ozone Loss and Validation Experiment (SOLVE), *J. Geophys. Res.*, 108,  
 698 doi:10.1029/2001JD002040, 2003.

699 Schoeberl, M. R., L. C. Sparling, C. H. Jackman, E. L. Fleming (2000), A Lagrangian  
 700 view of stratospheric trace gas distributions, *J. Geophys. Res.*, 105, 1537-1552.

701 Stolarski, R. S., A. R. Douglass, M. Gupta, P. A. Newman, S. Pawson, M. R. Schoeberl  
 702 and J. E. Nielsen (2006a), An ozone increase in the Antarctic summer

703 stratosphere: A dynamical response to the ozone hole, *Geophys. Res. Lett.*, **33**,  
704 doi:10.1029/2006GLO26820.

705 Stolarski, R. S., A. R. Douglass, S. Steenrod, and S. Pawson (2006b), Trends in  
706 stratospheric ozone: Lessons learned from a 3D chemical transport model, *J.*  
707 *Atmos. Sci.*, **63**, 1028-1041.

708 Strahan, S. E. and A. R. Douglass (2004), Evaluating the credibility of transport  
709 processes in simulations of ozone recovery using the Global Modeling Initiative  
710 three-dimensional model, *J. Geophys. Res.*, **109**, D05110,  
711 doi:10.1029/2003JD004238.

712 Volk, C. M., J. W. Elkins, D. W. Fahey, G. S. Dutton, J. M. Gilligan, M. Loewenstein, J.  
713 R. Podolski, K. R. Chan, and M. R. Gunson (2003), Evaluation of source gas  
714 lifetimes from stratospheric observations, *J. Geophys. Res.*, **102**, 25,543-25,564.

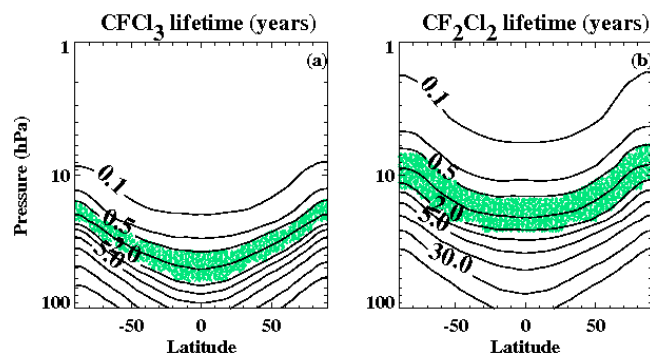
715 Waugh, D. W., S. E. Strahan, P. A. Newman (2007), Sensitivity of stratospheric  
716 inorganic chlorine to differences in transport, *Atmos. Chem. Phys.*, **7**, 4935-4941.

717 World Meteorological Organization (WMO) (1985), *Atmospheric Ozone 1985:*  
718 *Assessment of our Understanding of the Processes Controlling its present*  
719 *Distribution and Change, Rep. 16*, Global Ozone Research and Monitoring  
720 Project, Geneva

721 World Meteorological Organization (WMO) (2003), *Scientific assessment of ozone*  
722 *depletion: 2002, Rep. 47*, Global Ozone Research and Monitoring Project,  
723 Geneva.

724 World Meteorological Organization (WMO) (2007), *Scientific assessment of ozone*  
725 *depletion: 2006, Rep. 50*, Global Ozone Research and Monitoring Project,  
726 Geneva.  
727  
728

729



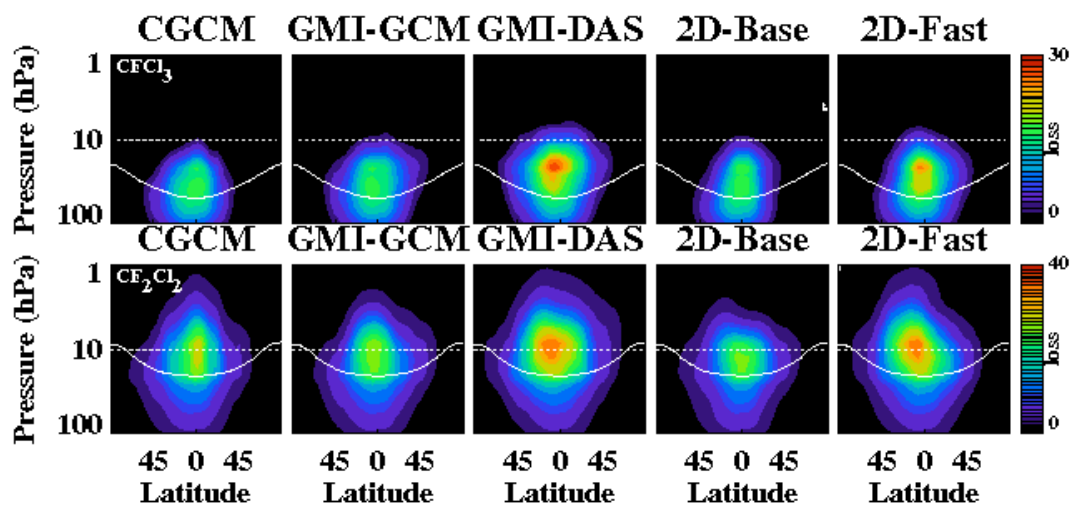
730

731 Figure 1 (a) Annual average local lifetimes as functions of latitude and altitude (pressure) for

732  $\text{CFCl}_3$ ; (b) same as a for  $\text{CF}_2\text{Cl}_2$ .

733

734



735

736 Figure 2 Loss rates ( $\text{\#}/\text{cm}^3/\text{s}$ ) for  $\text{CFCl}_3$  (top row) and  $\text{CF}_2\text{Cl}_2$  (bottom row) as functions of  
737 latitude and altitude. Results are shown for five separate simulations indicated by the titles. The  
738 white dashed line is the 10 hPa level. The white solid line shows where the local lifetime is 1  
739 year. In the tropics the maximum loss is just above this threshold.

740

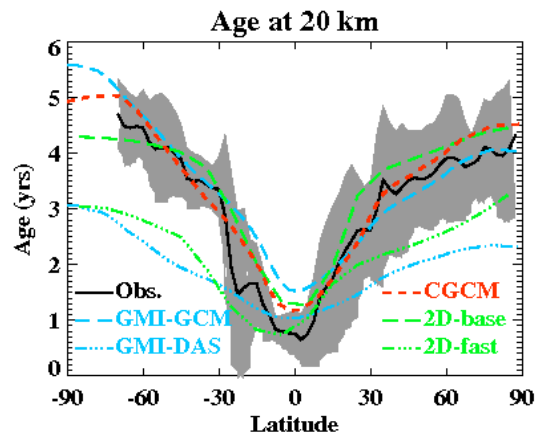


Figure 3: Age-of-air in the lower stratosphere from five simulations compared to data. The CGCM, 2D-base and GMI-GCM produce a distribution for the age of air that is similar to that observed; the GMI-DAS and 2D-fast ages are too young.

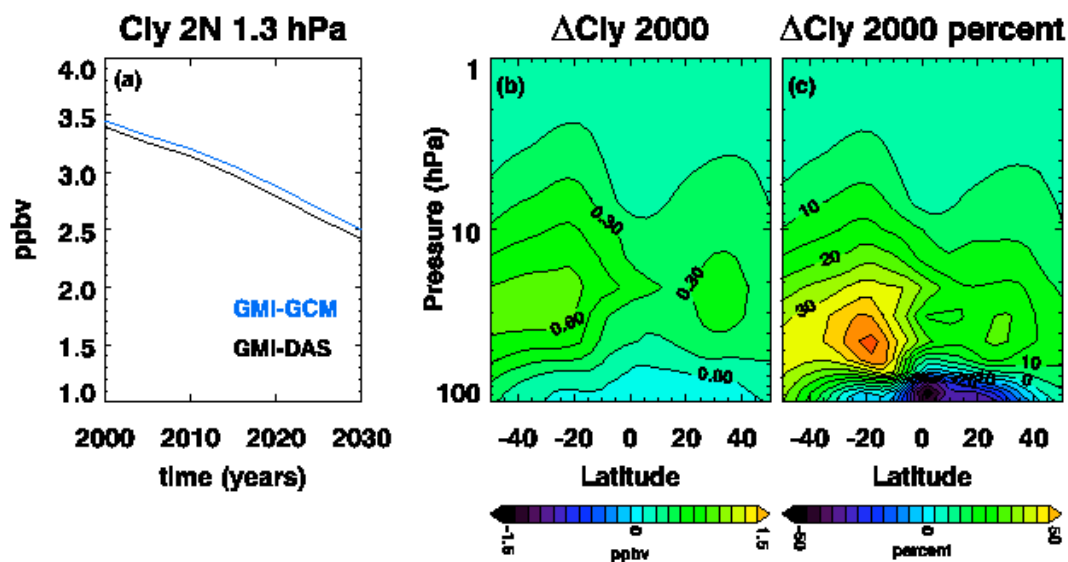


Figure 4(a) the  $\text{Cl}_y$  mixing ratios from GMI-GCM (blue) and GMI-DAS (black); (b) annual average difference (ppbv)  $\Delta\text{Cl}_y = \text{Cl}_y^{\text{GMI-GCM}} - \text{Cl}_y^{\text{GMI-DAS}}$ ; (c) same as (b) in percent.

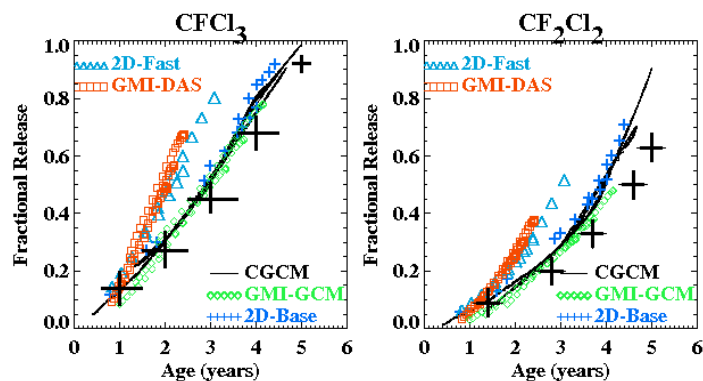


Figure 5 (a) The fractional release of  $\text{CFC13}$  relative to mean age from the simulations, northern hemisphere 50-70 hPa, and the range of values from aircraft observations (large crosses) taken from Figure 7 of Schauffler *et al.* [2003]; (b) same as (a) for  $\text{CF}_2\text{Cl}_2$ .

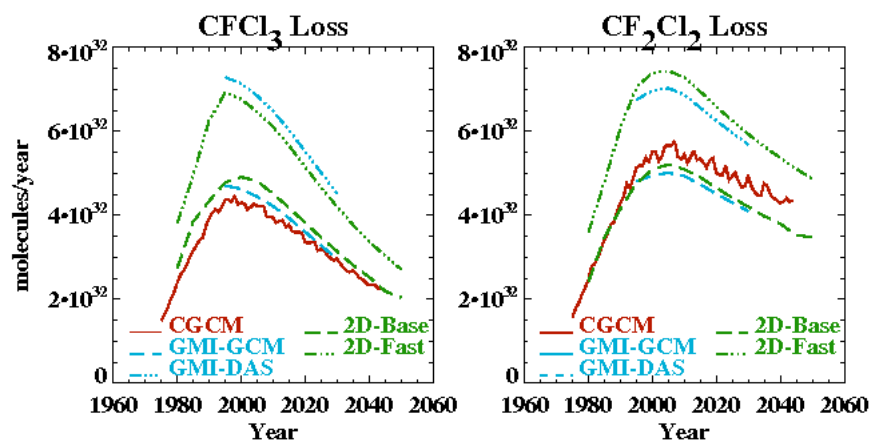
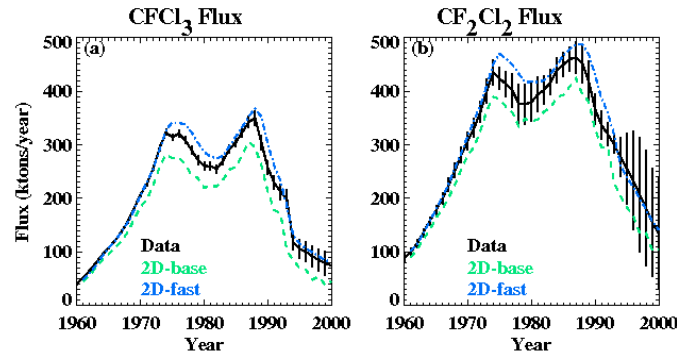


Figure 6 Annual-average loss for 1960 – 2060 for five simulations for (a)  $\text{CFC13}$  (b)  $\text{CF}_2\text{Cl}_2$ .

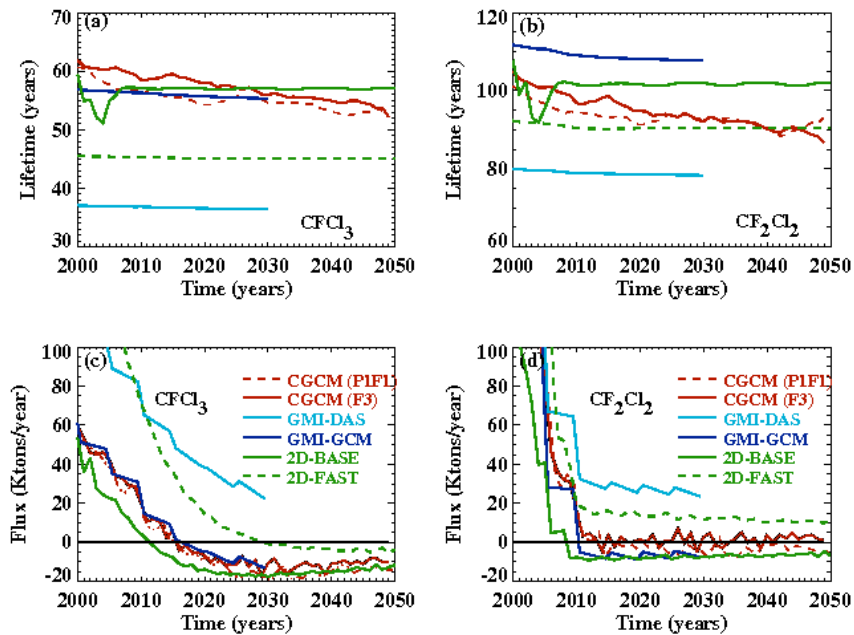
757



758

759 Figure 7(a) Computed fluxes of  $\text{CFCl}_3$  necessary to maintain the mixing ratio boundary  
 760 conditions applied to the 2D-base and 2D-fast simulations. The  $\text{CFCl}_3$  data are the bottom up  
 761 estimates of *McCullough et al.* [2001]; (b) same as (a) for  $\text{CF}_2\text{Cl}_2$ . The  $\text{CF}_2\text{Cl}_2$  data are taken  
 762 from *McCullough et al.* [2003].

763



764

765 Figure 8(a) Lifetime of  $\text{CFCl}_3$  calculated internally from the five simulations; (b) same as (a) for  
 766  $\text{CF}_2\text{Cl}_2$ ; (c) annual fluxes of  $\text{CFCl}_3$  implied by the annual change in the atmospheric burden and  
 767 annual loss for the five simulations; (d) same as (c) for  $\text{CF}_2\text{Cl}_2$ .

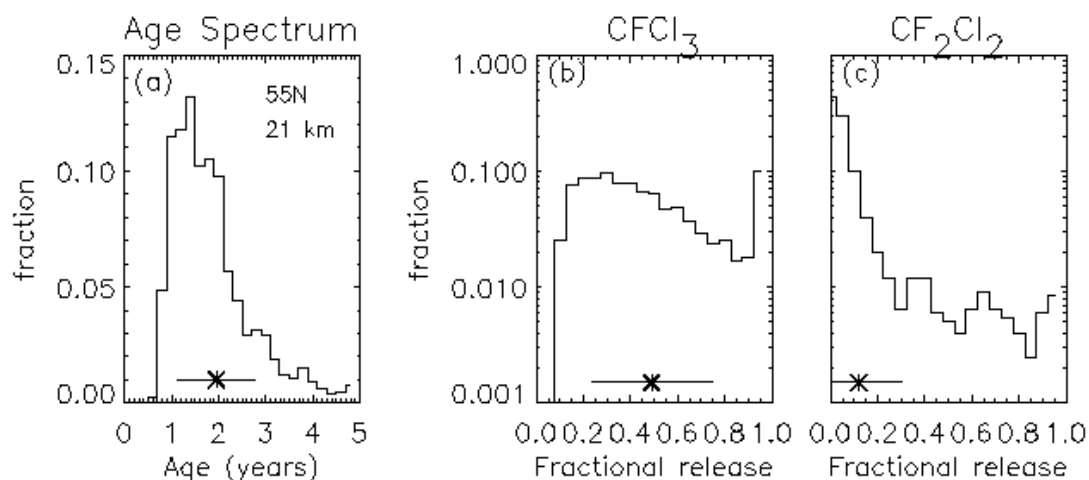


Figure 9(a) The age spectrum calculated using back trajectories from 55°N, 21 km; (b) the distribution of fractional release values for CFCl<sub>3</sub> calculated for the elements of the age spectrum; (c) same as (b) for CF<sub>2</sub>Cl<sub>2</sub>. On each panel the asterick is the mean value and the line is the standard deviation of the mean.

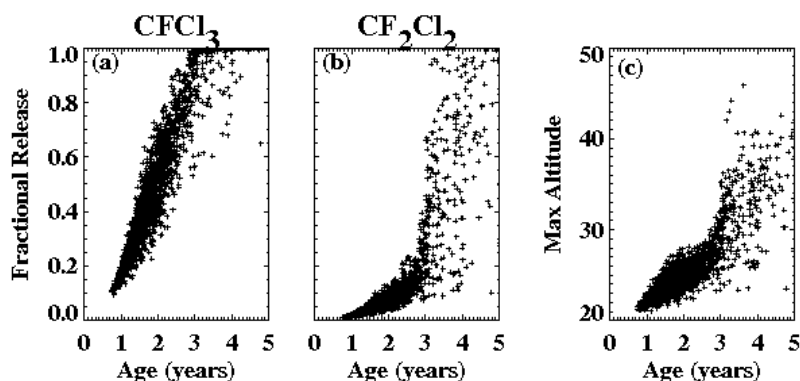
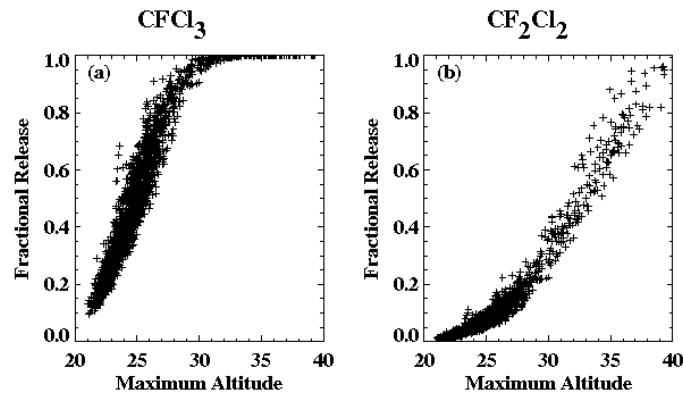


Figure 10 (a) The fractional release of CFCl<sub>3</sub> computed using back trajectories for each elements in the age spectrum; (b) same as (a) for CF<sub>2</sub>Cl<sub>2</sub>; (c) the maximum altitude along the trajectory for each element in the age spectrum.

780

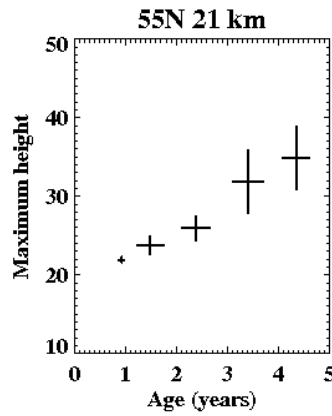


781

782

783 Figure 11 (a) The fractional release of  $\text{CFC}_{13}$  as a function of the maximum altitude along  
784 the trajectory; (b) same as (a) for  $\text{CFC}_{2\text{Cl}_2}$ .

785

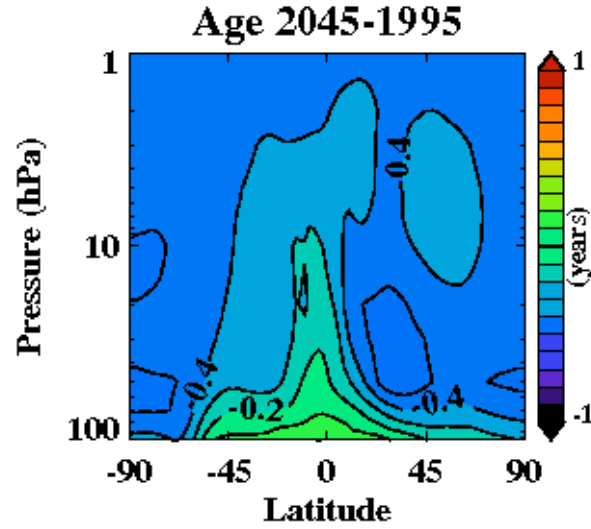


786

787 Figure 12 The mean maximum height and mean age for elements that are binned by age in single  
788 year intervals. The vertical and horizontal lines show the standard deviation of the maximum  
789 height and age respectively.

790

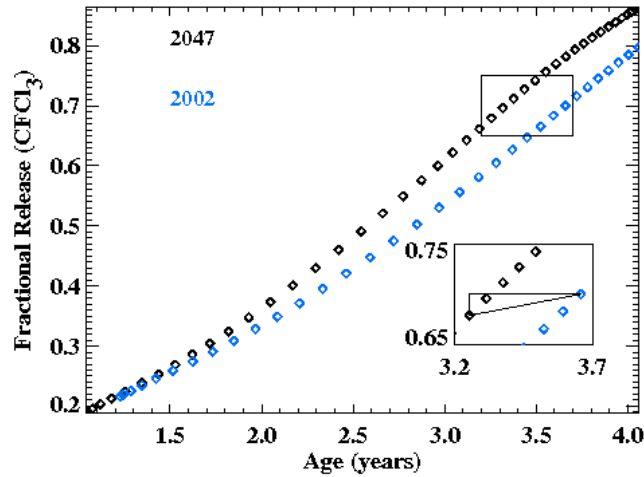
790



791

792 Figure 13: The annual average age-of air decreases throughout the stratosphere as shown by the  
793 difference between five-year averages centered on 2045 and 1995.

794



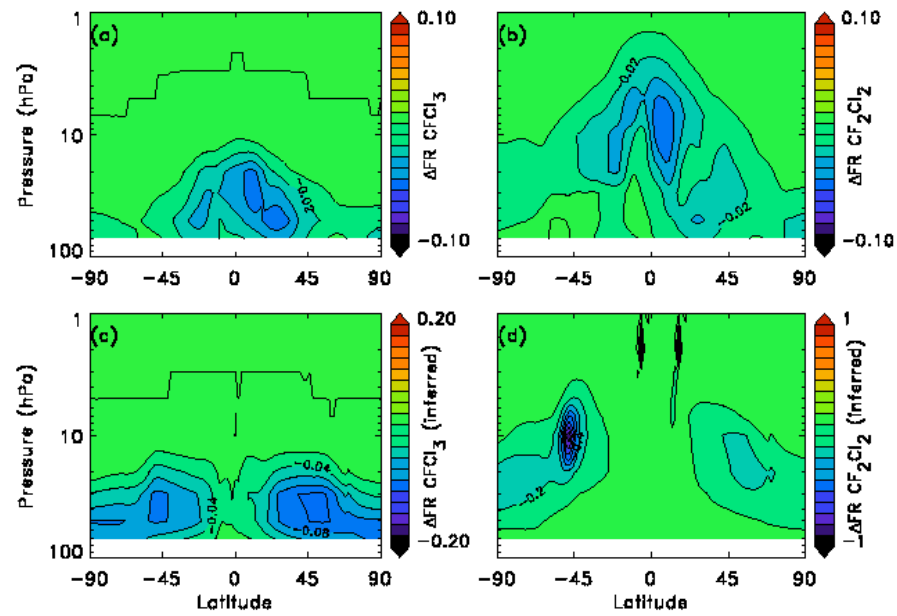
795

796 Figure 14: The relationship between mean age and fractional release changes as the residual  
797 circulation speeds up. The inset box magnifies the small unlabeled box to compare the change in  
798 age (x axis) with the change in fractional release (y axis) for 50°N, 50 hPa.

799

800

801



802

803 Figure 15(a) Changes in the fractional release distributions 2047 and 2002 for CFC1<sub>3</sub> as the  
 804 circulation speeds up; (b) same as (a) for CF<sub>2</sub>Cl<sub>2</sub>. (c) Change in fractional release if the 2002  
 805 relationship between CFC1<sub>3</sub> and mean age is unchanged; (d) same as (c) but for CF<sub>2</sub>Cl<sub>2</sub>.

806